

Identification of the Fusion Peptide-Containing Region in Betacoronavirus Spike Glycoproteins

Xiuyuan Ou,^a Wangliang Zheng,^a Yiwei Shan,^a Zhixia Mu,^a Samuel R. Dominguez,^b Kathryn V. Holmes,^c Zhaohui Qian^a

MOH Key Laboratory of Systems Biology of Pathogens, Institute of Pathogen Biology, Chinese Academy of Medical Sciences and Peking Union Medical College, Beijing, China^a; Department of Pediatrics^b and Department of Microbiology,^c University of Colorado School of Medicine, Aurora, Colorado, USA

ABSTRACT

The fusion peptides (FP) play an essential role in fusion of viral envelope with cellular membranes. The location and properties of the FPs in the spike (S) glycoproteins of different coronaviruses (CoV) have not yet been determined. Through amino acid sequence analysis of S proteins of representative CoVs, we identified a common region as a possible FP (pFP) that shares the characteristics of FPs of class I viral fusion proteins, including high Ala/Gly content, intermediate hydrophobicity, and few charged residues. To test the hypothesis that this region contains the CoV FP, we systemically mutated every residue in the pFP of Middle East respiratory syndrome betacoronavirus (MERS-CoV) and found that 11 of the 22 residues in the pFP (from G953 to L964, except for A956) were essential for S protein-mediated cell-cell fusion and virus entry. The synthetic MERS-CoV pFP core peptide (₉₅₅IAGVGWTAGL₉₆₄) induced extensive fusion of liposome membranes, while mutant peptide failed to induce any lipid mixing. We also selectively mutated residues in pFPs of two other β -CoVs, severe acute respiratory syndrome coronavirus (SARS-CoV) and mouse hepatitis virus (MHV). Although the amino acid sequences of these two pFPs differed significantly from that of MERS-CoV and each other, most of the pFP mutants of SARS-CoV and MHV also failed to mediate membrane fusion, suggesting that these pFPs are also the functional FPs. Thus, the FPs of 3 different lineages of β -CoVs are conserved in location within the S glycoproteins and in their functions, although their amino acid sequences have diverged significantly during CoV evolution.

IMPORTANCE

Within the class I viral fusion proteins of many enveloped viruses, the FP is the critical mediator of fusion of the viral envelope with host cell membranes leading to virus infection. FPs from within a virus family, like influenza viruses or human immunodeficiency viruses (HIV), tend to share high amino acid sequence identity. In this study, we determined the location and amino acid sequences of the FPs of S glycoproteins of 3 β -CoVs, MERS-CoV, SARS-CoV, and MHV, and demonstrated that they were essential for mediating cell-cell fusion and virus entry. Interestingly, in marked contrast to the FPs of influenza and HIV, the primary amino acid sequences of the FPs of β -CoVs in 3 different lineages differed significantly. Thus, during evolution the FPs of β -CoVs have diverged significantly in their primary sequences while maintaining the same essential biological functions. Our findings identify a potential new target for development of drugs against CoVs.

Viruses are obligate intracellular parasites, and host cell membranes act as a barrier to virus entry. Enveloped viruses initiate infection of cells through fusion of the viral and cellular membranes. CoVs are enveloped and single-stranded plus-sense RNA viruses that cause a variety of diseases among many different species (1). Phylogenetically, CoVs are divided into four genera: alphacoronavirus (α -CoV), betacoronavirus (β -CoV), gammacoronavirus (γ -CoV), and deltacoronavirus (δ -CoV) (2).

CoVs enter cells through the interactions of the viral S proteins with host receptors. Several cellular proteins have been identified as receptors for their respective CoVs. Specific examples include human angiotensin-converting enzyme 2 (hACE2) for severe acute respiratory syndrome coronavirus (SARS-CoV) and human CoV NL63 (3, 4), human dipeptidyl peptidase IV (hDPP4) for Middle East respiratory syndrome betacoronavirus (MERS-CoV) (5), bat DPP4 for bat CoV HKU4 (6), human aminopeptidase N (hAPN) for human CoV 229E (7), and mouse carcinoembryonic antigen-related cell adhesion molecule 1a (mCEACAM1a) for mouse hepatitis virus (MHV) (8).

The CoV S protein is a class I viral fusion protein. On the CoV virions, the 180- to 200-kDa S proteins are found as trimers. S monomers contain two subunits, called S1 and S2. S1 contains the

receptor binding domain (RBD) and is responsible for receptor recognition and binding, whereas S2 possesses the membrane fusion machinery (9, 10), including a fusion peptide (FP), two heptad repeat domains (called the N-terminal and C-terminal heptad repeats, HR-N and HR-C), the juxtamembrane domain (JMD), and a transmembrane domain (TMD) (Fig. 1A).

To mediate membrane fusion, S protein must be activated, which requires both proteolytic cleavage (priming) and receptor binding with or without pH change (triggering) (11–13). Several host priming proteases are important for S protein-mediated CoV

Received 4 January 2016 Accepted 23 March 2016

Accepted manuscript posted online 30 March 2016

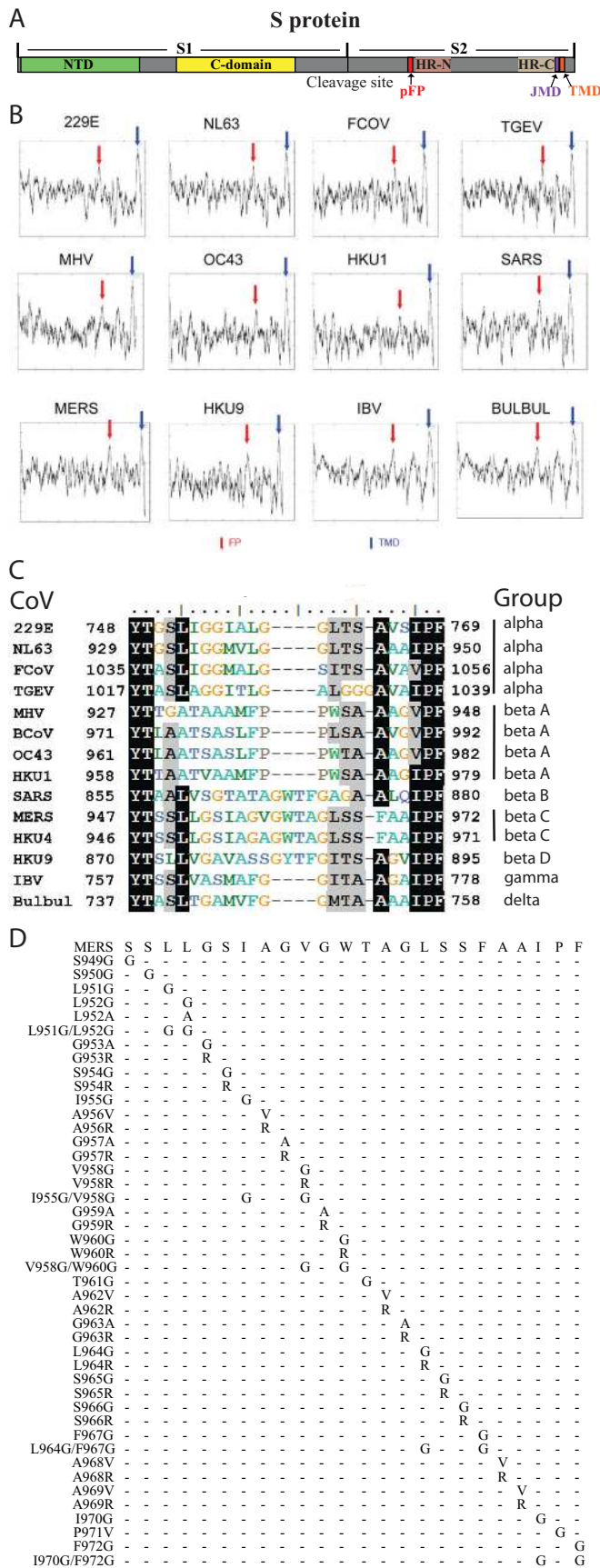
Citation Ou X, Zheng W, Shan Y, Mu Z, Dominguez SR, Holmes KV, Qian Z. 2016. Identification of the fusion peptide-containing region in betacoronavirus spike glycoproteins. *J Virol* 90:5586–5600. doi:10.1128/JVI.00015-16.

Editor: S. Perlman, University of Iowa

Address correspondence to Zhaohui Qian, zqian2013@sina.com.

X.O. and W.Z. contributed equally to this study.

Copyright © 2016, American Society for Microbiology. All Rights Reserved.



entry, including cathepsin B and L, serine proteases TMPRSS2 and TMPRSS4, trypsin, elastase, human airway trypsin-like protease (HAT), and furin (14–20). S protein activation leads to a series of conformational changes and insertion of a putative FP into target membrane, an essential step in membrane fusion and virus infection. Class I viral fusion proteins generally contain one FP, located either internally, like the FPs of the glycoprotein (GP) of Ebola virus and the envelope protein (Env) of avian sarcoma leukosis virus (ASLV) (21–24), or immediately downstream of the “priming” site, as seen in the hemagglutinin (HA) of influenza virus and the Env protein of HIV (25, 26). Although the primary sequences and lengths of FPs vary significantly among different class I viral fusion proteins, they share several common features. Most are rich in Ala and/or Gly, have an intermediate level of hydrophobicity with membrane binding potential, form helical structures in the presence of trifluoroethanol (TFE), and contain very few charged residues in the middle of their sequences (13, 25, 27).

Although significant efforts have been made to locate the FPs of different CoVs (28–35), the exact locations and sequences of CoV FPs remains controversial. While Chambers et al. predicted that the CoV FP likely was adjacent to HR-N (35), Madu et al. proposed that the sequence immediately following a critical and conserved trypsin cleavage site at the arginine of position 797 (R797) of SARS-CoV S protein, SFIEDLLFNKVTLADAGF, may be the FP of SARS-CoV S protein (32). In this study, we used bioinformatics to identify a 17- to 22-amino-acid-long region, just upstream of HR-N, in S2 of different CoVs with characteristic features of the FPs of other class I viral fusion proteins. Using mutational, biochemical, and biophysical analyses of this region of the S proteins of 3 β -CoVs, MERS-CoV, SARS-CoV, and MHV, we provide data to support this region as the functional FP of CoV S proteins.

MATERIALS AND METHODS

Cell culture. HEK-293, 293T, HEK-293 cells stably expressing hACE2 (293/hACE2), HeLa cells stably expressing hDPP4 (HeLa/hDPP4), and HeLa cells stably expressing mouse CEACAM1a (HeLa/mCEACAM1a) were maintained in Dulbecco’s modified Eagle’s medium (DMEM) (Invitrogen, Carlsbad, CA) supplemented with 10% fetal bovine serum (FBS) and 2% penicillin-streptomycin-amphotericin B (Fungizone; Invitrogen) at 37°C with 5% CO₂.

Constructs and mutagenesis. The constructs, pcDNA-SARS-CoV SΔ19 (36), pcDNA-MERS-CoV SΔ16 (37), and pcDNA-MHV S (38), have been described previously. Briefly, DNA encoding codon-optimized SARS-CoV S protein lacking the last 19 amino acids (aa), MERS-CoV S protein lacking the last 16 aa but with a FLAG tag at the C terminus, or full-length MHV S protein was cloned between BamHI and NotI sites of pcDNA3.1. All SARS-CoV, MERS-CoV, and MHV S mutants were derived from the plasmids pcDNA-SARS-CoV SΔ19, pcDNA-MERS-CoV SΔ16, and pcDNA-MHV S, respectively. All mutagenesis experiments were carried out using a Q5 mutagenesis kit (NEB, MA, USA). After the entire coding sequences were verified by sequencing, the BamHI- and

FIG 1 pFPs of CoVs. (A) Diagram of CoV spike protein. NTD, N-terminal domain; C-domain, C-terminal domain; Cleavage site, protease cleavage site separating S1 and S2; pFP, possible fusion peptide; HR-N, N-terminal heptad repeat; HR-C, C-terminal heptad repeat; JMD, juxtamembrane domain; TMD, transmembrane domain. (B) Locations of pFPs and TMDs of S proteins of representative CoVs predicted by TMPred. (C) Amino acid sequence alignment of the pFPs of different CoVs. (D) Summary of the amino acid substitutions made in the pFP of MERS-CoV S protein.

NotI-containing mutated S gene was cloned back into pcDNA3.1. A plasmid encoding full-length hACE2 (pACE2-cq) was kindly provided by M. Farzan (Scripps Research Institute, Florida campus). A plasmid encoding full-length human DPP4 (pcDNA-hDPP4) was purchased from Sino Biological Inc. (Beijing, China). A plasmid encoding full-length mouse CEACAM1a (mCEACAM1a) has been described previously (39). To express soluble human ACE2 (shACE2) and soluble human DPP4 (shDPP4), DNA fragments encoding residues 19 to 615 of human hACE2 with N-terminal 6His and FLAG tags and residues 40 to 766 of human DPP4 with C-terminal 6His and AVI tags were cloned between Sall and HindIII and between BamHI and XhoI of modified pFASTBac1 vector with gp67 signal peptide, respectively. To express soluble mouse CEACAM1a (smCEACAM1a), residues 1 to 236 of mCEACAM1a with C-terminal 6His and AVI tags were cloned into EcoRI and NotI of pFASTBac1. These soluble receptors were expressed in High Five insect cells using the Bac-to-Bac system (Invitrogen) and purified using nickel affinity and ion-exchange chromatography.

Analysis of S protein expression on cell surfaces. Briefly, HEK-293T cells were transfected with 2 μ g of either wild-type (WT) or mutant S protein-expressing plasmid using polyethylenimine (PEI) (Polysciences Inc., Warrington, PA, USA). Forty hours later, cells were detached from plates by incubating with phosphate-buffered saline (PBS) plus 1 mM EDTA for 5 min at 37°C. After washing, cells were incubated with the respective primary anti-S antibody for 1 h on ice. The primary antibodies for SARS-CoV S Δ 19, MERS-CoV S Δ 16, and MHV S protein were rabbit polyclonal anti-SARS S1 antibody (1:300 dilution) (Sinobiological Inc., Beijing, China), mouse monoclonal anti-MERS S antibody (1:300 dilution) (Sinobiological Inc., Beijing, China), and goat polyclonal anti-MHV S antibody (AO4) (1:200 dilution), respectively. After washing, cells were stained with Alexa Fluor 488-conjugated goat anti-rabbit IgG (1:200) (ZSGB-Bio LLC, Beijing, China) for SARS S, goat anti-mouse IgG (1:200) (ZSGB-Bio LLC, Beijing, China) for MERS S, or rabbit anti-goat IgG (1:200) (ZSGB-Bio LLC, Beijing, China) for MHV S. After washing, cells were fixed with 1% paraformaldehyde and analyzed by flow cytometry.

Binding of soluble receptor. HEK-293T cells were transfected with plasmids encoding either wild-type or mutant S proteins with PEI. After 40 h, cells were lifted with PBS plus 1 mM EDTA and immediately washed twice with PBS plus 2% normal donkey serum (NDS). About 2×10^5 cells were incubated with 1 μ g of shACE2, shDPP4, or smCEACAM1a for 1 h on ice. After washing, cells were incubated with mouse monoclonal anti-FLAG M2 antibody (1:1,000 dilution) (Sigma, St. Louis, MO, USA) for shACE2, followed by Alexa Fluor 488-conjugated goat anti-mouse IgG (1:200) or rabbit polyclonal anti-AVI antibody (1:200 dilution) (Shanghai Enzyme-Linked Biotechnology Co., Shanghai, China) for shDPP4 and smCEACAM1a, and finally with Alexa Fluor 488-conjugated goat anti-rabbit IgG (1:200). Cells were fixed with 1% paraformaldehyde and analyzed by flow cytometry.

Production and transduction of S protein-pseudotyped lentiviruses. Pseudovirions with spike proteins were produced as described previously (40), with minor modifications. Briefly, plasmids encoding either wild-type or mutant S proteins were cotransfected into 293T cells with pLenti-Luc-green fluorescent protein (GFP) (a gift from Fang Li, Duke University) and psPAX2 (Addgene, Cambridge, MA) at a molar ratio of 1:1:1 by using PEI. The following day, the cells were fed with fresh medium. After 24 h of incubation, the supernatant media containing pseudovirions were centrifuged at $800 \times g$ for 5 min to remove debris and passed through a 0.45- μ m filter. To quantify S protein-mediated entry of pseudovirions, susceptible cells were seeded at about 25 to 30% confluence in 24-well plates. The following day, cells were inoculated with 500 μ l of 1:1 diluted viruses. At 40 h postinoculation (p.i.), cells were lysed at room temperature with 120 μ l of medium with an equal volume of Steady-Glo (Promega, Madison, WI). Transduction efficiency was monitored by quantitation of luciferase activity using a Modulus II microplate reader (Turner Biosystems, Sunnyvale, CA). All experiments were done in triplicate and repeated at least three times.

Detection of viral spike glycoproteins by Western blotting. To evaluate S protein expression in cells, HEK 293T cells were transfected with plasmids encoding either wild-type or mutant S proteins by using PEI. Forty hours later, cells were lysed with lysis buffer (50 mM Tris-HCl, pH 7.4, 150 mM NaCl, 2 mM EDTA, 1% Triton X-100, 0.1% SDS) containing protease inhibitors (Roche, USA). To determine S protein incorporation into pseudotype virions, the virion-containing supernatant was pelleted through a 20% sucrose cushion at 30,000 rpm at 4°C for 2 h in a Beckman SW41 rotor (40). Viral pellets were resuspended in PBS. Cell lysates and pseudovirion pellets were separated on a 4 to 15% SDS-PAGE and transferred to a nitrocellulose blot. The SARS-CoV S Δ 19, MERS-CoV S Δ 16, and MHV S proteins were detected with polyclonal rabbit anti-SARS S1 antibodies (1:2,000), monoclonal mouse anti-MERS S antibody (1:1,000), and polyclonal goat anti-MHV S antibody (1:2,000), respectively. The blots were further stained with the horseradish peroxidase-conjugated antibodies goat anti-rabbit IgG (1:10,000), goat anti-mouse IgG (1:10,000), and rabbit anti-goat IgG (1:10,000), respectively, and visualized with Clarity Western ECL substrate (Bio-Rad, Hercules, CA, USA). The β -actin and HIV capsid protein (p24) were detected using mouse monoclonal anti- β -actin antibody (1:5,000) (Sigma, St. Louis, MO, USA) and rabbit polyclonal anti-p24 antibody (1:5,000) (Sinobiological Inc., Beijing, China), respectively.

Cell-cell fusion assays. Cell-cell fusion assays were performed as previously described (37), with modifications. Briefly, 293T cells were cotransfected with plasmids encoding CoV S glycoprotein and GFP. Forty hours later, cells were detached with trypsin (0.25%) and overlaid on a 70% confluent monolayer of 293/hACE2, HeLa/hDPP4, or HeLa/mCEACAM1a cells at a ratio of approximately one S-expressing cell to two receptor-expressing cells. After overnight incubation, images of syncytia were captured with a Nikon TE2000 epifluorescence microscope running MetaMorph software (Molecular Devices). To quantify S protein-mediated cell-cell fusion, 293T cells cotransfected with pFR-Luc, which contains a synthetic promoter with five tandem repeats of the yeast GAL4 binding sites that controls expression of the luciferase gene, plasmid encoding S protein, and the receptor-expressing cells (293/hACE2, HeLa/hDPP4, or HeLa/mCEACAM1a) were transfected with pBD-NF- κ B, which encodes a fusion protein with the DNA binding domain of GAL4 and transcription activation domain of NF- κ B. The following day, S-expressing 293T cells were lifted with trypsin and overlaid onto receptor-expressing cells at a ratio of about one S-expressing cell to two receptor-expressing cells. When cell-cell fusion occurred, luciferase expression would be activated through binding of the GAL4-NF- κ B fusion protein to GAL4 binding sites at the promoter of the luciferase gene. After 24 h of incubation, cells were lysed by adding 120 μ l of medium with an equal volume of Steady-Glo, and luciferase activity was measured with a Modulus II microplate reader. All experiments were done in triplicate and repeated at least three times.

Peptide synthesis. All peptides were synthesized using a standard solid-phase Fmoc (9-fluorenylmethoxy carbonyl) method by Scilight Biotechnology LLC (Shanghai, China). Purification was carried out by reverse-phase high-performance liquid chromatography (HPLC) and verified by mass spectrometry. An Ahx-KKK linker was added to all peptides used in circular dichroism (CD) spectroscopy analysis to increase peptide solubility in PBS. The following peptides were used for CD analysis: CTRL, KWGQYTNSPFLTKGF-Ahx-KKK (a control peptide from a previous SARS study [33]); HIV FP (41), AVGIGALFLGFLGAAG-Ahx-KKK; and MERS pFP, SLLGSIAGVGTAGLSSFAAI-Ahx-KKK. The following peptides were used for the lipid mixing study: CTRL, KWGQYTNSPFLTKGF; HIV FP, AVGIGALFLGFLGAAG; MERS short FP (sFP), IAGVGWTAGL; MERS mutant FP (mFP), IAGRGRTAGL (letters in bold indicate mutations).

CD spectroscopy. CD spectroscopy analysis was performed to study the secondary structure of fusion peptides in increasing trifluoroethanol (TFE) concentrations. CD spectra were acquired on a Jasco J-815 spectropolarimeter (Jasco, Tokyo, Japan) using a 1-nm bandwidth with a 1-nm

step resolution from 195 to 260 nm at room temperature. Spectra were corrected by the subtraction of its respective solvent. The sample spectrum was smoothed with a Savitsky-Golay filter. The α -helical content was estimated from the ellipticity value at 222 nm, $[\theta]_{222}$, according to the empirical equation of Chen et al. (42): percent helical content = $100 \times \{[\theta]_{222} / -395,000 \times (1 - 2.57/n)\}$, where n is the number of peptide bonds.

Preparation of liposomes. Equimolar amounts of egg phosphatidylethanolamine (PE), egg phosphatidylcholine (PC), and cholesterol (Avanti Polar Lipids, Alabaster, AL, USA) were dried from chloroform into a thin film by constant flow of nitrogen gas and rehydrated in Tris buffer (10 mM Tris, 150 mM NaCl, 0.1 mM EDTA, pH 7.2) at a concentration of 10 mM. Large unilamellar vesicles (LUV) were prepared by the extrusion procedure (43). Briefly, after 10 freeze-thaw cycles, liposomes were extruded 21 times through two stacked polycarbonate membranes with a pore size of 0.1 μ m using an Avanti mini-extruder. Liposome with 0.6% (molar ratio) fluorescent resonance energy transfer (FRET) pairs Rho-PE and NBD-PE (Thermo Fisher) were prepared in the same way.

Lipid mixing. Lipid mixing was determined using the resonance energy transfer assay as described by Struck et al. (44), with minor modifications. Briefly, Rho-PE- and NBD-PE-labeled liposomes were mixed with unlabeled liposomes at a ratio of 1:9. The final lipid concentration was 300 μ M. Specified amounts of various peptides were added to initiate fusion, and changes in fluorescence were monitored at 535 nm with the excitation wavelength set at 465 nm and a slit width of 4 nm using Fluoromax-4 (Horiba, Paris, France). The initial residual fluorescence of the labeled and unlabeled vesicles was set up as the baseline for 0% fluorescence value (f_0); 100% fluorescence value (f_{100}) was achieved by addition of Triton X-100 to a final concentration of 0.2%. The extent of lipid mixing was calculated using the following formula: $\%f_t = (f_t - f_0) / (f_{100} - f_0) \times 100$, where f_t is the fluorescence value observed after addition of fusion peptide at time t .

RESULTS

During membrane fusion, the FP of S protein inserts into the host membranes. We reasoned that CoV FPs might share some common properties with the transmembrane domains (TMD) and that the location of the FP within the S protein might be predictable by using TMD prediction software programs. The FPs of HIV-1 Env and influenza virus HA have been studied extensively, and their locations and amino acid sequences are known. As a proof of concept, we first tested whether TM software programs could accurately identify the FPs of HIV-1 Env and influenza H1N1 HA proteins. Both the FPs and TMDs of HIV-1 Env and influenza HA were accurately identified by two software programs, TMpred (http://www.ch.embnet.org/software/TMPRED_form.html) and TMHMM (<http://www.cbs.dtu.dk/services/TMHMM/>) (data not shown). Subsequently, we applied these two software programs to analyze S proteins of a wide variety of CoVs. The positions of the TMDs of the S proteins of all CoVs studied were correctly identified by both software programs (Fig. 1B). In addition, both of these TMD prediction programs identified another region consistently flanked by YT at the N terminus and PF at the C terminus in all of the S proteins of the CoVs tested (Fig. 1B and C). Although the primary amino acid sequences of this region were not conserved in all of the CoVs studied, they were all Ala or Gly rich, relatively hydrophobic, and contained no charged residues, characteristics shared by the FPs of other class I viral fusion proteins (Fig. 1C). We named this region in CoV S proteins the possible FP (pFP).

To investigate if the pFP is the functional fusion peptide of CoVs, we selected the S protein of MERS-CoV, a lineage C β -CoV, as an example. The MERS-CoV pFP contains amino acids 949 to

970 (Fig. 1C). Individual and occasionally double amino acid substitutions were introduced at each position of pFP (Fig. 1D). First, we determined if any of the mutations altered the expression of S protein in 293T cells. Consistent with our previous report (37), two bands around 200 kDa were detected in the cell lysate of 293T cells expressing wild-type (WT) S protein, likely reflecting the different glycosylation of full-length S proteins during transport through the Golgi apparatus. However, the cell lysate also contained a significant proportion of S protein cleaved between S1 and S2, around 100 kDa, which was absent from our previous report but previously reported by the Pohlmann laboratory (45). The difference between that study and our earlier report likely resulted from different culture conditions, especially sera and media from different vendors. Among the 44 total G, A, V, or R substitutions, 30 (S949G, S950G, L952A, G953A, G953R, S954G, S954R, I955G, A956V, A956R, G957A, G957R, V958G, V958R, I955G/V958G, G959A, G959R, W960G, W960R, V958G/W960G, T961A, A962V, A962R, G963A, G963R, L964G, L964R, S965G, S966G, and A968V) showed no or minor effects on S protein expression or processing compared to the WT (Fig. 2A and Table 1). In contrast, 14 substitutions (L951G, L952G, L951G/L952G, S965R, S966R, F967G, L964F/F967G, A968R, A969V, A969R, I970G, P971V, F972G, and I970G/F972G) showed significant reductions in S protein expression and changes in patterns of S protein processing (Fig. 2A and Table 1). The cleaved S protein species were almost absent from corresponding cell lysates, suggesting that these residues (L951, L952, S965, S966, F967, A968, A969, I970, P971, and F972) are important for S protein folding and processing.

We then investigated if any amino acid substitutions in the pFP influenced transport of the S protein to the cell surface. The 293T cells expressing WT or mutant S proteins were incubated on ice with mouse monoclonal anti-MERS-CoV S protein antibody and analyzed by flow cytometry. The same 30 mutants that showed WT levels of S protein expression in cell lysates also showed WT levels of S protein on the cell surface (Fig. 2B and Table 1). As expected, the mutants with defects in S protein expression and processing also showed only low levels of S proteins on the cell surface.

Although the pFP is located within the MERS-CoV S2 subunit, amino acid substitutions in pFP might affect S protein binding to its cognate receptor, hDPP4, by altering the overall conformation of the S protein. To determine whether or not any amino acid substitution in pFP changed S protein binding to hDPP4, we used V5-tagged soluble hDPP4 (shDPP4) to bind 293T cells transiently expressing WT or pFP mutant S proteins of MERS-CoV. The percentage of cells that bound shDPP4 and the level of shDPP4 bound to S protein were quantitated by flow cytometry. The same 30 mutant S proteins that showed WT levels of expression on cell surfaces also bound to shDPP4 at levels similar to those of WT S protein (Fig. 3 and Table 1), indicating that these pFP mutations had no effect on receptor binding.

Because the fusion peptide is essential for S protein-mediated membrane fusion, we then explored whether any mutation in pFP altered MERS-CoV S protein-mediated cell-cell fusion. To more easily visualize cell-cell fusion or syncytia, the 293T cells expressing S protein were cotransfected with a GFP-expressing plasmid and then overlaid with HeLa/hDPP4 cells in the presence of trypsin. Consistent with our previous report (37), WT MERS-CoV S protein induced very large syncytia (Fig. 4), and syncytium for-

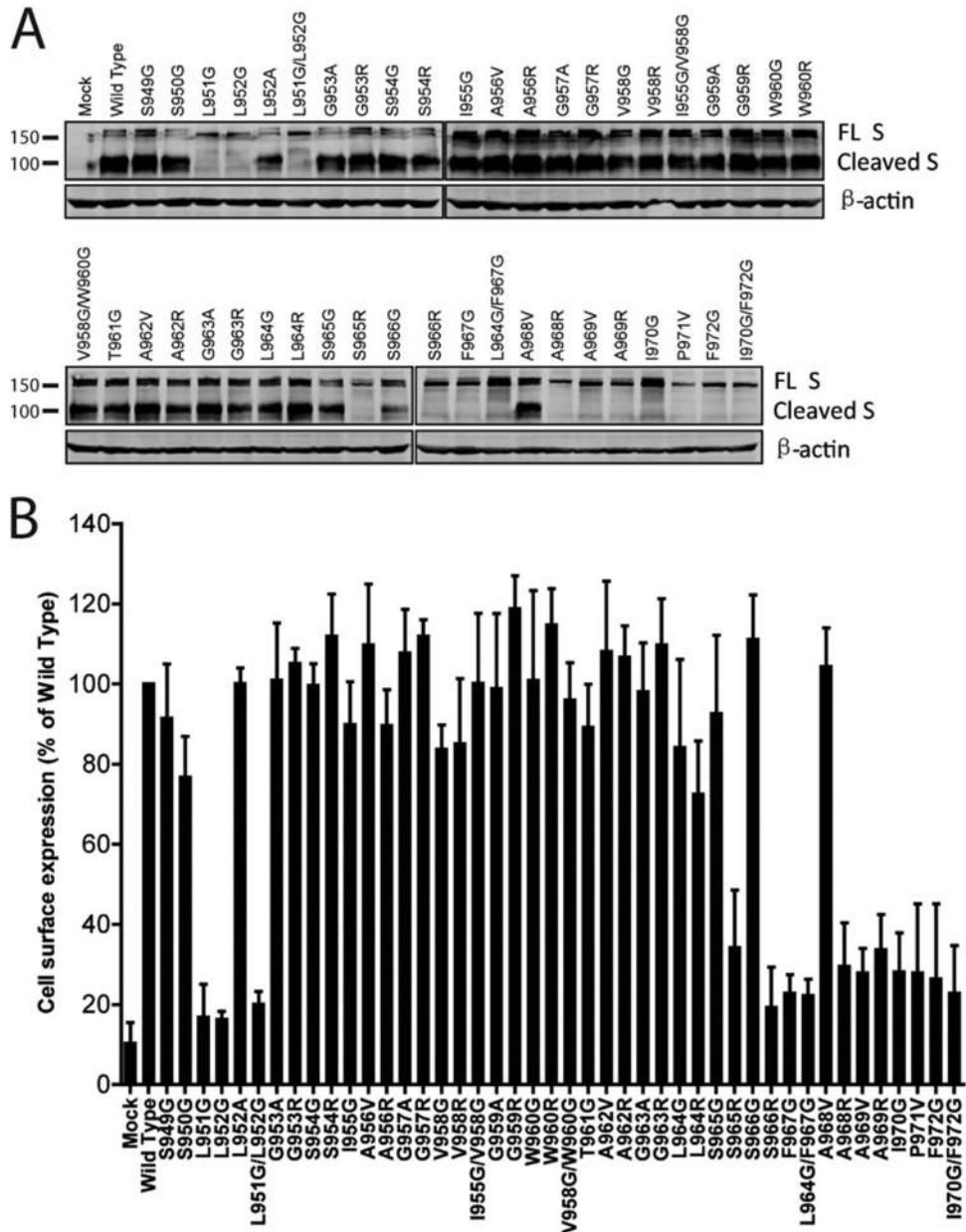


FIG 2 Analysis of expression of pFP mutants of MERS-CoV S protein in 293T cells. (A) Western blot analysis of expression of WT or mutant MERS S protein in cell lysate. The MERS S protein was detected by using mouse monoclonal anti-MERS S antibody; β -actin was detected with mouse monoclonal anti-actin antibody. FL, full length. (B) Analysis of surface expression of mutant MERS-CoV S protein by flow cytometry. MERS-CoV S protein-expressing 293T cells were stained with mouse monoclonal anti-MERS S antibody. The amount of wild-type S protein on cell surfaces was set as 100%. All of the experiments shown were repeated at least three times.

mation depended on the availability of hDPP4 (data not shown). Among 30 pFP S protein mutants that were expressed well, transported to the cell surface efficiently, and bound to hDPP4 at levels similar to the WT, 14 mutants (S949G, S950G, G953A, S954G, A956V, A956R, G957A, V958G, G959A, A962V, G963A, L964G, S965G, and A968V) induced large syncytia in HeLa/hDPP4 cells similar to the WT, 12 mutants (G953R, S954R, I955G, G957R, V958R, I955G/V958G, W960R, V958G/W960G, T961G, A962R, G963R, and L964R) induced little or no syncytium formation, and 4 mutants (L952A, G959R, W960G, and S966G) induced syncytia of much smaller size than the WT (Fig. 4). These results indicate

that these 13 residues, L952, G953, S954, I955, G957, V958, G959, W960, T961, A962, G963, L964, and S966, in MERS-CoV S protein are critical for S protein-mediated, receptor-dependent membrane fusion that would lead to virus infection.

To quantify the effect of amino acid substitutions on S protein-mediated syncytium formation, we utilized a luciferase-based quantification assay from a yeast two-hybrid system from Stratagene-Agilent Technologies, Inc. Compared to mock transfection and parental HeLa cell controls, fusion of 293T cells expressing WT MERS-CoV S proteins with HeLa/hDPP4 cells increased luciferase activity by about 1,000-fold (Fig. 5). The overall pattern of

TABLE 1 Summary of pFP mutants of betacoronaviruses

β -CoV	Expression in cell lysate ^a	Expression on cell surface ^b	Incorporation in virion ^c	Receptor binding	Cell-cell fusion ^d	Pseudovirion transduction ^d
MERS wild type	+++	+++	+++	+++	+++	+++
S949A	+++	+++	+++	+++	+++	+++
S950G	+++	+++	+++	+++	+++	+++
L951G	+	–	–	–	–	–
L952G	+	–	–	–	–	–
L952A	++	+++	++	+++	++	+
L951G/L952G	+	–	–	–	–	–
G953A	+++	+++	++	+++	+++	+
G953R	+++	+++	++	+++	–	–
S954G	+++	+++	+++	+++	+++	+++
S954R	+++	+++	+++	+++	–	–
I955G	+++	+++	+++	+++	–	–
A956V	+++	+++	+++	+++	++	+++
A956R	+++	+++	+++	+++	+++	+++
G957A	+++	+++	+++	+++	+++	++
G957R	+++	+++	+++	+++	–	–
V958G	+++	+++	+++	+++	+++	+++
V958R	+++	+++	+++	+++	–	–
I955G/V958G	+++	+++	+++	+++	–	–
G959A	+++	+++	+++	+++	+++	+++
G959R	+++	+++	+++	+++	+	–
W960G	+++	+++	+++	+++	+	+
W960R	+++	+++	+++	+++	–	–
V958G/W960G	+++	+++	+++	+++	–	–
T961G	+++	+++	+++	+++	–	–
A962V	+++	+++	+++	+++	+++	+++
A962R	+++	+++	+++	+++	+	–
G963A	+++	+++	+++	+++	++	++
G963R	+++	+++	++	+++	–	–
L964G	+++	+++	+++	+++	+++	++
L964R	+++	+++	+++	+++	–	–
S965G	+++	+++	+++	+++	+++	+++
S965R	+	+	+	+	–	–
S966G	++	+++	+	++	+++	+
S966R	+	–	–	+	–	–
F967G	+	+	–	+	–	–
L964G/F967G	+	+	–	+	–	–
A968V	+++	+++	+++	++	+++	++
A968R	+	+	–	+	–	–
A969V	+	+	–	+	+	–
A969R	+	+	+	+	–	–
I970G	+	+	+	+	–	–
P971V	+	+	–	–	–	–
F972G	+	+	–	–	–	–
I970G/F972G	+	+	–	–	–	–
SARS wild type	+++	+++	+++	+++	+++	+++
W868R	+++	ND	+++	ND	+	–
W868G	+++	+++	+++	+++	++	+++
F870R	+++	ND	+++	ND	+	–
F870G	+++	+++	+++	+++	++	+++
W868G/F870G	+++	+++	+++	+++	–	–
L876R	+++	ND	+++	ND	–	–
L876G	+++	+++	+++	+++	++	+
I878R	++	ND	++	ND	–	–
I878G	++	+++	++	+++	+	–
L876G/I878G	++	+++	++	+++	–	–
MHV wild type	+++	+++	+++	+++	+++	+++
M963R	+	+	++	++	+	–

(Continued on following page)

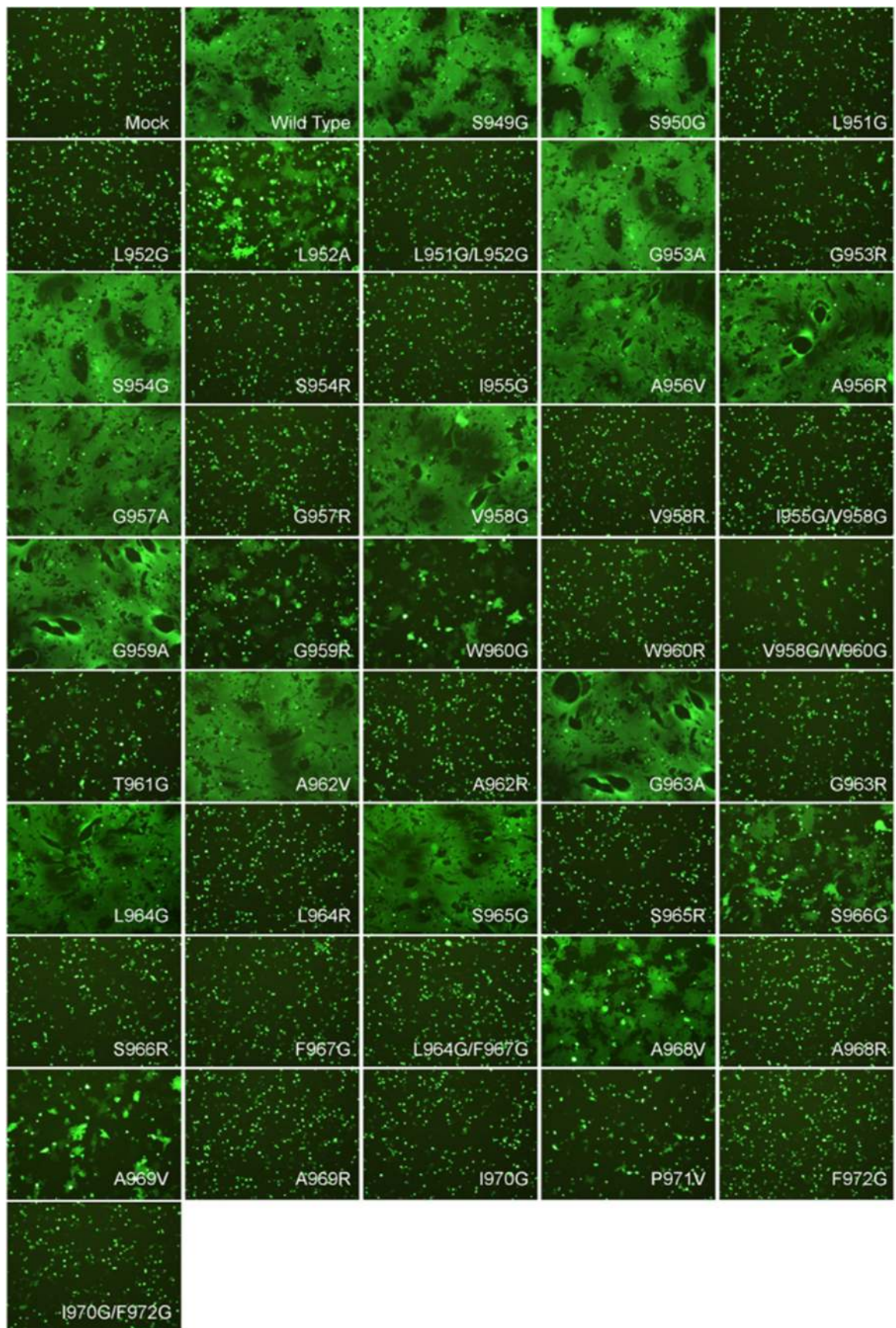


FIG 4 Cell-cell fusion mediated by WT or mutant MERS-CoV S protein. MERS-CoV S protein-expressing 293T cells were transiently transfected with eGFP and then incubated with HeLa/hDPP4 cells overnight in the presence of trypsin.

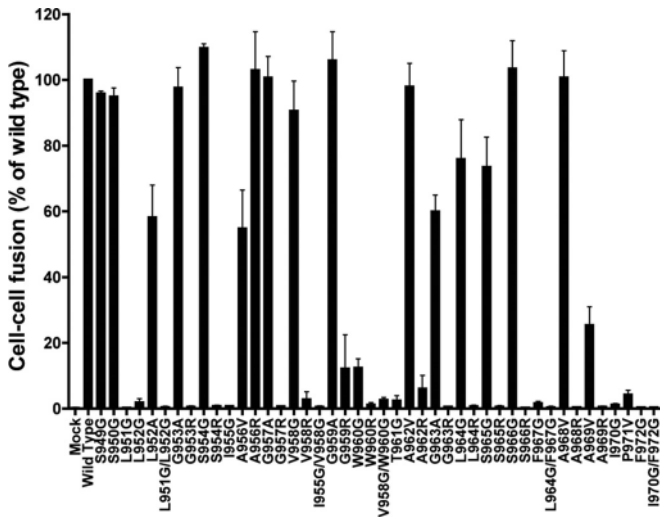


FIG 5 Quantitative analysis of syncytium formation mediated by WT or mutant MERS-CoV S protein. Cell-cell fusion was quantified by measurement of luciferase activities. Typically, the relative luciferase activities from cell-cell fusion induced by wild-type S protein were over 10⁷, while the reading for the mock control was less than 1,000. The experiments were done at least three times.

dent manner, whereas the negative-control peptide did not induce any significant lipid mixing. Moreover, when we replaced V958 and W960, two residues essential for cell-cell fusion and virus entry, with Arg in the MERS-CoV sFP peptide, the resulting mutant FP (mFP) (₉₅₅IAGRGRTAGL₉₆₄; letters in bold indicate mutations) failed to induce any noticeable lipid mixing, confirming that these two residues are essential for lipid mixing.

Having established the essential roles in membrane fusion and virus entry of the pFP of the S protein MERS-CoV, a β -CoV in group C, we also investigated the functional role of the pFPs of other CoVs. After examining the alignment of the pFPs of different CoVs (Fig. 1B), we selected the pFPs of the S proteins of SARS-CoV, a lineage B β -CoV, and MHV, a lineage A β -CoV, for functional study. While the pFP of SARS-CoV and the pFP of MERS-CoV share the same length and have sequence identity in about 1/3 of their amino acids, the pFP of MHV differs markedly from that of MERS-CoV in both length and amino acid sequence. Since hydrophobic residues in the pFP of MERS-CoV play important roles in membrane fusion, we selected W868, F870, L876, and I878 of SARS-CoV S protein and M936, F937, P938, P939, and W940 of MHV S protein for further analysis. Single Arg and/or Gly substitutions were introduced into the MHV and SARS-CoV S proteins at these positions.

With the exception of I878-related mutants, the pFP mutant S proteins of SARS-CoV were expressed well (data not shown), bound well to its receptor, hACE2, at levels similar to that of the WT (data not shown), and were incorporated into pseudovirions efficiently (Fig. 8B). I878 mutants (I878G, I878R, and the double mutant L876G/I878G) were expressed slightly less well in cell lysates (data not shown) and showed reduced S protein incorporation into pseudovirions (Fig. 8B), indicating that I878 plays a role in folding and transport of S protein. Similar to MERS-CoV S protein, all Arg mutations in pFP of SARS-CoV effectively abolished S protein-mediated cell-cell fusion and virus entry (Fig. 8A and C and Table 1), suggesting that these residues are indeed es-

essential for membrane fusion. Compared to Arg mutations, Gly substitutions in the pFP of SARS S protein had less effect on cell-cell fusion and virus entry. Interestingly, although the single mutants W868G and F870G showed an almost WT level of infection, the double mutant W868G/F870G abolished S protein-mediated virus entry (Fig. 8A), confirming that these two residues in S protein of SARS-CoV are important for membrane fusion.

All MHV S protein pFP with single Arg substitutions (M936R, F937R, P938R, P939R, and W940R) showed significant reduction in both S-mediated pseudovirion entry (Fig. 8D and Table 1) and cell-cell fusion (Fig. 8F and Table 1). S proteins with M936R substitutions, however, showed significantly decreased expression of S protein in cell lysate (data not shown) and incorporation into pseudovirions (Fig. 8E). This may partly explain why M936R mutations had detrimental effects on virus infection and cell-cell fusion. P938R substitution also showed a slight reduction in expression and virion incorporation of S protein. In contrast, S proteins with F937R, P939R, and W940R substitutions had wild-type levels of S protein expression (data not shown) and incorporation into virions (Fig. 8E) and binding to its cognate receptor (data not shown), mCEACAM1a, but failed to mediate virus entry or syncytium formation. These data indicate that F937, P939, and W940 in the pFP are essential for MHV S protein-mediated membrane fusion.

DISCUSSION

Proteolytic priming is one of the early essential steps required to activate the fusion potential of class I viral fusion proteins, and is believed to release the restraint on the viral FP leading to exposure of the FP. The proteolytic priming sites for most of the class I viral fusion proteins are either immediately proximal to or not far upstream of the viral FP (21–26). Therefore, identifying the key proteolytic priming site may lead to discovery of a viral FP. However, in the case of CoVs, the priming sites are less clear. In an attempt to identify the trypsin cleavage site essential for MERS-CoV S protein-mediated trypsin-dependent entry, we mutated several trypsin sites (R884G/R887G, K897G, R921G, and K933G) upstream of the N terminus of HR-N of MERS-CoV S protein (48, 49). Surprisingly, we found that none of these sites was essential for trypsin-primed MERS-CoV S protein-mediated virus entry (data not shown). Therefore, there might be built-in redundancy of trypsin priming sites within the MERS-CoV S protein such that cleavage by trypsin might occur at multiple sites, and single cleavage at any one of these sites might be sufficient to prime the MERS-CoV S protein.

Since there was not a single essential trypsin priming site for the S protein of MERS-CoV, we used an alternative approach to look for the FP of MERS-CoV S protein. Using TMpred and TMHMM software programs to analyze the S2 domains of a variety of CoVs, we identified a region in S2 that is flanked by YT at the N terminus and PF at the C terminus and is found in all of the CoVs studied (Fig. 1B and C). This pFP region has characteristics of the known FPs of other class I viral fusion proteins, Gly or Ala rich, relatively hydrophobic, and without charged residues. This pFP region is located at about 7 to 23 amino acids upstream of the N terminus of HR-N of CoV S proteins, depending on where the N terminus of HR-N was proposed (48–53). Mutagenesis analysis on the pFPs of MERS-CoV, SARS-CoV, and MHV S proteins revealed that this region was essential for S protein-mediated syncytium formation and virus entry (Table 1) and strongly support the idea that the

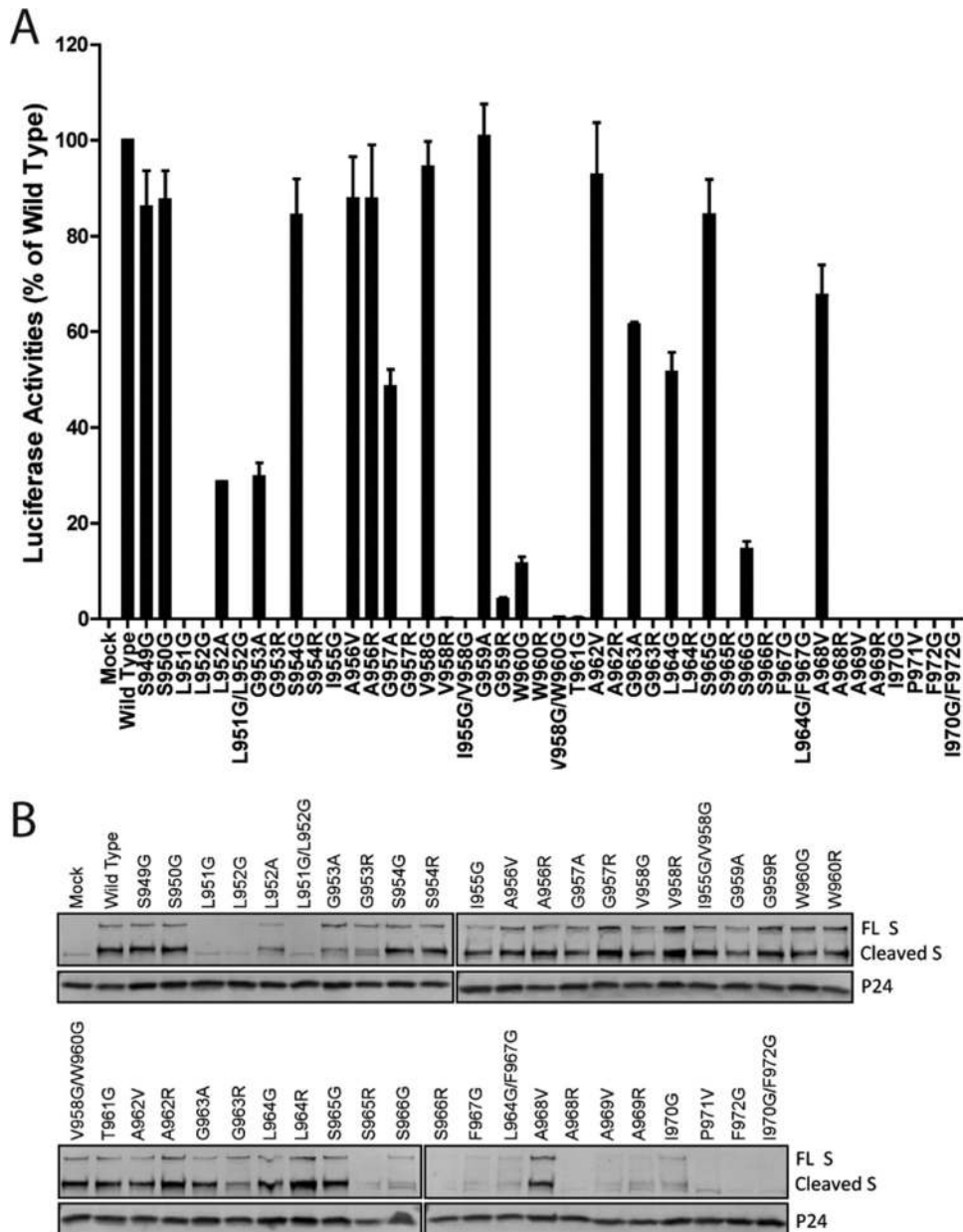


FIG 6 Entry of pseudotype virions with wild-type or mutant MERS S protein. (A) Entry of pseudovirions with wild-type or mutant MERS-CoV S proteins into HeLa/hDPP4 cells. Pseudovirus entry was quantitated by luciferase activity at 40 h postinoculation. A typical transduction by wild-type S protein pseudoviruses resulted in a more than 10,000-fold increase of luciferase activity. The experiments were repeated at least three times, and an average from three experiments is shown. (B) Detection of wild-type or mutant S protein incorporation into pseudovirions by Western blot analysis. MERS S protein was detected using mouse monoclonal anti-MERS S antibody; p24, a gag protein of HIV, was detected using rabbit polyclonal anti-p24 antibodies. FL S, full-length S protein. The experiments were repeated twice and a representative is shown.

pFP of β -CoV S protein is the functional viral fusion peptide. This conclusion is further strengthened by our findings that the synthetic pFP of MERS-CoV S protein formed an α -helix in the presence of TFE and its core short sequence, called sFP, mediated membrane fusion of liposome efficiently (Fig. 7), which are characteristics of FPs of other class I viral fusion proteins (13). Our results are also consistent with previous biophysical studies on synthetic peptides from SARS-CoV S protein (29, 33) and previous studies in MHV showing that P939 may be critical for membrane fusion and virus infection (54, 55).

About one-third of the residues located at the C terminus of the pFP of MERS-CoV S protein appear to play important roles in the stability and processing of the S protein, since the introduction of amino acid substitutions into these positions significantly reduced S protein expression, processing, and incorporation into pseudotyped virions. Residues close to the C terminus of the pFP of the SARS-CoV S protein also appear to be important for S protein folding, as replacement of I878 with R or G also decreased S protein expression and incorporation into virions. However, this region might also be important for membrane fusion mediated by S

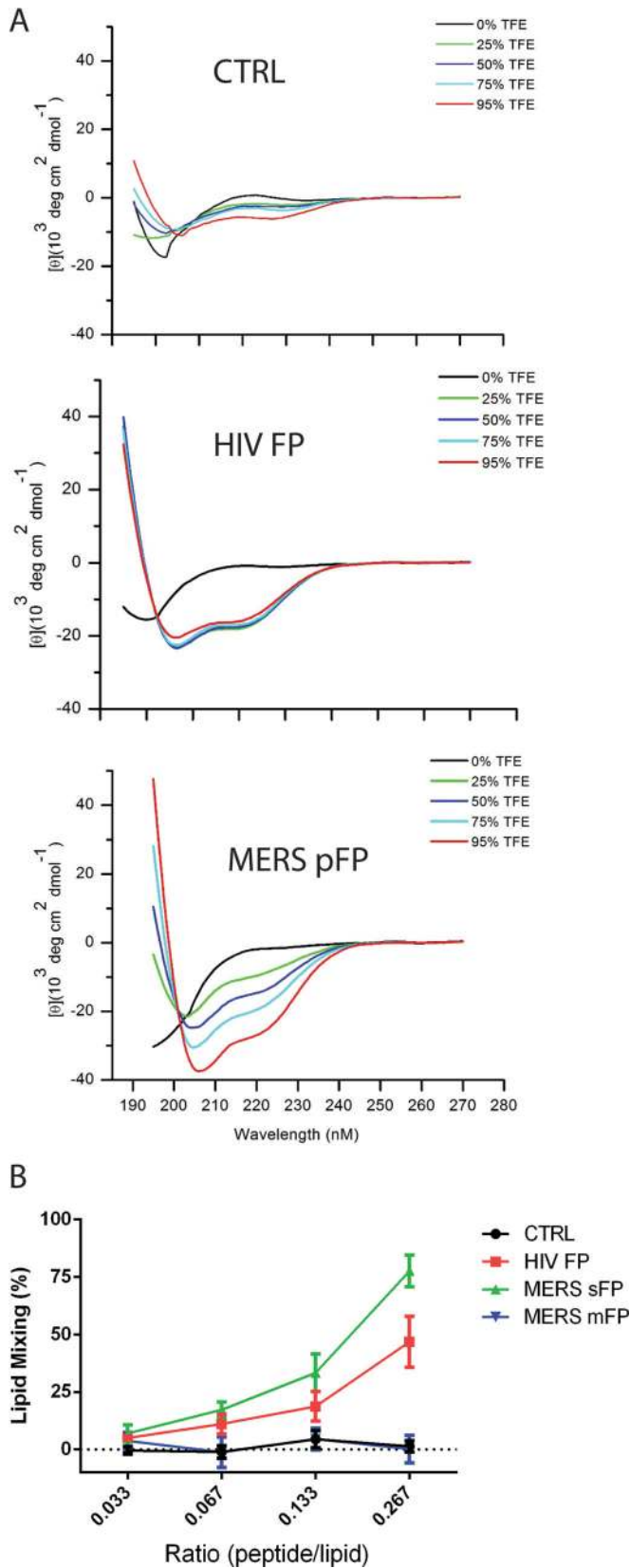


FIG 7 Biophysical analysis of synthetic pFP peptide of MERS-CoV. (A) CD analysis of secondary structure of pFP of MERS-CoV S protein. CTRL, KWGQYTNSPFLT-KGF-Ahx-KKK (a control peptide from a previous

protein. A recent study on SARS-CoV by Liao et al. (56) raised the possibility that this region has direct interactions with the JMD in S protein during membrane fusion.

Among the amino acid substitutions that we introduced into the pFP of MERS-CoV S protein, Arg had a more profound effect on the function of the pFP of MERS-CoV S protein than Gly, Ala, or Val. Compared to Gly, Ala, and Val, Arg is positively charged and its side chain is significantly longer than those of Gly, Ala, or Val; hence, Arg substitution represents a more dramatic change than these amino acids. Moreover, Arg substitution may cause a higher free-energy barrier for insertion of FP into membrane (57). Although the exact mechanism(s) of how these substitutions in the pFP abrogate membrane fusion requires further investigation, there are several possibilities. Introduction of mutation(s) into the pFP of MERS-CoV S protein might distort the structure of FP required for membrane fusion similar to G1V and W14A mutations of the FP of influenza HA (58–60). Alternatively, the substitutions might change how the FP inserts into membranes (61–63) or affect the oligomerization of the FPs that is important for membrane fusion (64, 65).

Recent studies in influenza virus HA (66), paramyxovirus F protein (67), and HIV Env (68) reveal that many viral FPs interact and oligomerize with their TMDs in the lipid, which promotes lipid mixing and membrane fusion. Whether the FP and TMD of CoV S protein interact with each other during membrane fusion remains to be determined. Interestingly, the primary amino acid sequences of the TMDs among different CoVs also do not share high identity (Fig. 9). Of note, there is a GXXXG or (small)XXX(small) motif (G, Gly; small, Ala, Gly, or Ser; X, any residue) present in all of the pFPs of CoVs. These motifs were initially discovered in human glycoprotein A and subsequently have been implicated in TMD interactions of more than 20 proteins (69). Recent studies in influenza HA and HIV Env have suggested that such GXXXG motifs also play an important role in FP-FP or FP-TMD interaction (66, 68, 70). There are two GXXXG motifs, GSIAG and GWTAG, within the FP of MERS-CoV. Replacement in MERS-CoV S protein of any one of these four Gly residues (G953, G957, G959, or G963) with Arg abrogated the membrane fusion activity of the viral protein. However, whether these GXXXG motifs in the pFP of MERS S protein are essential for oligomerization or interaction with the TMD requires further investigation.

FPs of some class I viral fusion proteins, like HIV Env and influenza HA, share high identity in primary amino acid sequence within each virus family. In marked contrast, this study found no strong amino acid sequence identity among the pFPs of MERS-CoV, SARS-CoV, and MHV. The lengths of the FPs of these three different lineages of β -CoV also differ significantly, ranging from

SARS-CoV peptide study [33]); HIV FP, AVGIGALFLGFLGAAG-Ahx-KKK; MERS pFP, SLLGSIAGVGTAGLSSFAAI-Ahx-KKK. All peptides were dissolved in PBS, and their CD spectra were measured in the presence of the indicated concentration of TFE. Experiments were done twice, and one representative is shown. (B) Lipid mixing induced by synthetic pFP of MERS-CoV S protein. LUVs were made with equimolar amounts of PE, PC, and cholesterol. The extent of lipid mixing was determined by monitoring the changes in fluorescence intensity at 535 nm at 37°C upon addition of peptide. Each data point is averaged from three independent experiments, and error bars represent standard deviations of the means. CTRL, KWGQYTNSPFLT-KGF; HIV FP, AVGIGALFLGFLGAAG; MERS sFP, IAGVGTAGL; MERS mFP, IAGRRTAGL.

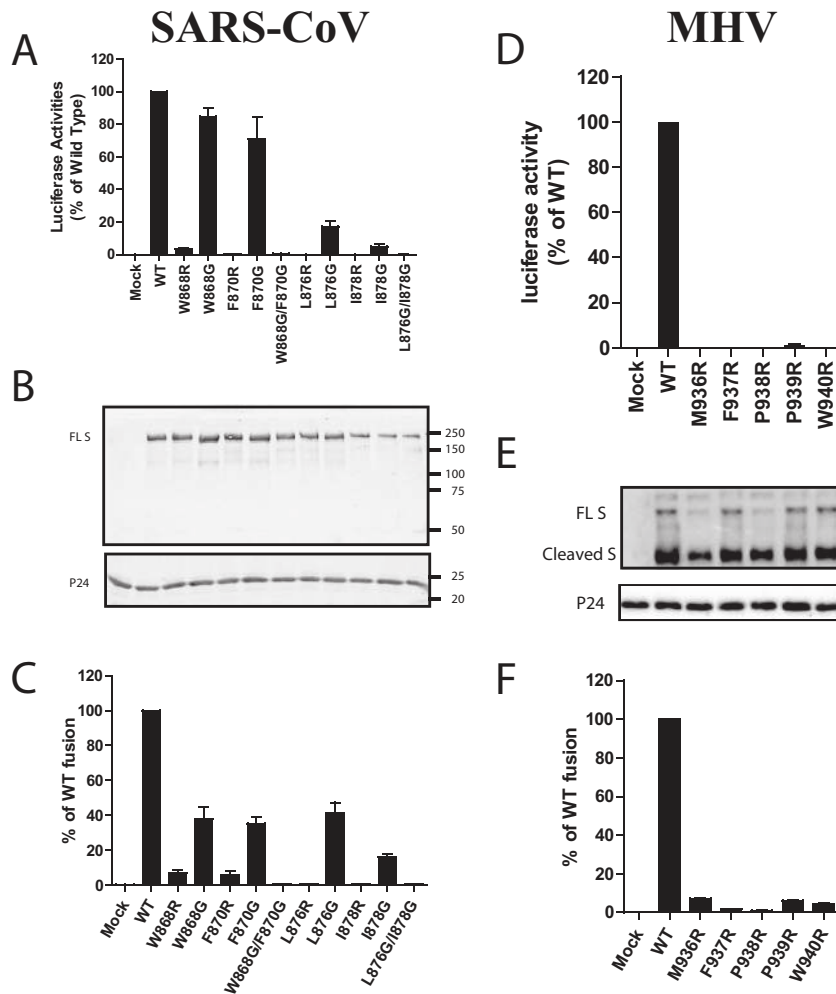


FIG 8 Effects of mutations at the pFPs of SARS-CoV and MHV on pseudovirus transduction and cell-cell fusion. (A and D) Entry of wild-type or mutant SARS-CoV S protein pseudovirions into 293/hACE2 cells (A) or MHV S protein pseudovirions into HeLa/mCEACAM1a cells (D). Pseudovirus entry was quantitated by luciferase activity at 40 h postinoculation. The experiments were repeated at least three times, and averages from three experiments are shown. (B and E) Detection of wild-type or mutant S protein of SARS-CoV (B) or MHV (E) incorporation into pseudovirions by Western blot analysis. SARS S protein was detected using rabbit polyclonal anti-SARS S1 antibody, MHV S protein was detected using goat polyclonal anti-MHV S antibody AO4, and p24, a gag protein of HIV, was detected using rabbit polyclonal anti-p24 antibodies. The experiments were repeated at least three times, and one representative is shown. (C and F). Cell-cell fusion mediated by mutant SARS (C) or MHV (F) S proteins. Experiments were performed as described in the legend to Fig. 3B, except that 293/hACE2 cells were used as targets for SARS-CoV S protein (C) and HeLa/mCEACAM1a cells were used as targets for MHV S protein (F). An average from three experiments is shown.

18 amino acids for MHV to 22 amino acids for MERS-CoV and SARS-CoV (Fig. 1B). Within each lineage of β -CoVs, the pFPs appear to be better conserved (Fig. 1B). Although underlying mechanism(s) causing the amino acid sequence divergence of FPs of different lineages of β -CoVs remains to be determined, CoV RNA-dependent RNA polymerase error, recombination, and selective pressure during evolution likely contribute to these changes. Previous study of MHV persistent infection in DBT cells showed that accumulation of mutations in fusion peptide and HR-N could lead to extending host range (55). The lack of conservation of the pFP amino acid sequences, however, is not unique for CoVs, as FPs from different paramyxoviruses also lack high identity in their primary amino acid sequences (67).

As an internal fusion peptide, how does the activated FP of CoVs fold and mediate membrane fusion? Recent studies have demonstrated that FPs from different class I viral fusion proteins

might adapt different conformations to mediate membrane fusion. Depending on the lipid composition, the FPs of HIV-1 Env and parainfluenza virus F proteins can fold as either an α -helix (67, 71) or β -sheet (65, 72), and both can be fusogenic. In contrast, the overall conformation of the FPs of Ebola virus GP and influenza virus HA is α -helical in the presence of TFE, but they fold as hairpin-like structures or “knuckle” conformations when they insert into their target membranes (63, 73). Sequence analysis of the S proteins of different CoVs (Fig. 1B) shows the presence in the pFPs of a Gly-Gly (GG) motif in α -, γ -, and δ -CoVs or a Pro-Pro (PP) motif in β -CoVs in lineage A. GG and PP motifs favor the formation of turn or hairpin structures, which suggests that the FPs of some CoVs also adapt a hairpin-like structure when inserting into host membranes. In the FPs of SARS-CoV and MERS-CoV in β -CoV groups b and c, respectively, however, neither a GG nor a PP motif is present. Of note, the FP from group 2

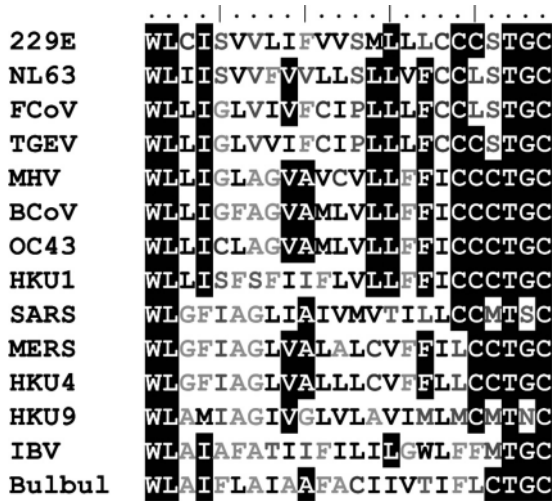


FIG 9 Alignment of TMDs of S proteins of representative CoVs.

influenza virus HA also lacks a central GG or PP motif but instead forms a hairpin-like structure with G13 at the turn with a Trp and a hydrophilic residue immediately following G13 (74). Interestingly, a similar motif is also present in the pFPs of SARS-CoV and MERS-CoV (Fig. 1B).

While all known class III viral fusion proteins have two fusion loops, all known class I viral fusion proteins except for CoV S protein only have a single fusion peptide. In the case of CoVs, in addition to pFP found in this study, Madu et al. previously found a highly conserved region in SARS-CoV S protein essential for membrane fusion and proposed it as the fusion peptide (32), although this sequence lacks some common features of FPs of other class I viral fusion proteins, including high Ala/Gly content. Their proposed FP is about 80 amino acids away from the N terminus of HR-N (50, 52) and about 40 amino acids upstream of the N terminus of our pFP. The possibility of the presence of two fusion peptides in the S protein of CoV is very intriguing. How these two possible fusion peptides collaborate to mediate membrane fusion requires further investigation.

In summary, using a bioinformatics approach we have identified a region in the S proteins of CoVs that has several properties of the FPs of several classical class I viral fusion proteins. Further molecular biological, biochemical, and biophysical analyses demonstrated that this region is essential for receptor-dependent membrane fusion mediated by S proteins of several β -CoVs in different lineages, strongly suggesting that it is the functional FP of these and likely other CoVs. These findings will provide significant clues for future studies of the membrane fusion mechanism of CoVs and may provide a new target for drugs against CoV infections.

ACKNOWLEDGMENTS

This work was supported by grants from Chinese Science and Technology Key Projects (2014ZX10004001), the National Natural Science Foundation of China (31470266), MOHRSS of China (9019005), and the Institute of Pathogen Biology, CAMS (2014IPB101 and 2015IPB301), to Z.Q. This work was also supported by the PUMC Youth Fund and by Fundamental Research Funds for the Central Universities (3332013118), as well as by the Program for Changjiang Scholars and Innovative Research Team in University (IRT13007).

FUNDING INFORMATION

This work, including the efforts of Zhaohui Qian, was funded by Chinese Science and Technology Key Projects (2014ZX10004001). This work, including the efforts of Zhaohui Qian, was funded by National Natural Science Foundation of China (NSFC) (31470266).

REFERENCES

1. Masters PS, Perlman S. 2013. Coronaviridae, p 825–858. *In* Knipe DM, Howley PM, Cohen JL, Griffin DE, Lamb RA, Martin MA, Racaniello VR, Roizman B (ed), *Fields virology*, 6th ed, vol 1. Lippincott Williams & Wilkins, Philadelphia, PA.
2. King AMQ, Adams MJ, Carstens EB, Lefkowitz EJ (ed). 2011. Virus taxonomy. Classification and nomenclature of viruses. Ninth report of the International Committee on Taxonomy of Viruses. Elsevier Academic Press, San Diego, CA. <http://ictvonline.org/virusTaxonomy.asp?version=2011>.
3. Hofmann H, Pyrc K, van der Hoek L, Geier M, Berkhout B, Pohlmann S. 2005. Human coronavirus NL63 employs the severe acute respiratory syndrome coronavirus receptor for cellular entry. *Proc Natl Acad Sci U S A* 102:7988–7993. <http://dx.doi.org/10.1073/pnas.0409465102>.
4. Li W, Moore MJ, Vasilieva N, Sui J, Wong SK, Berne MA, Somasundaran M, Sullivan JL, Luzuriaga K, Greenough TC, Choe H, Farzan M. 2003. Angiotensin-converting enzyme 2 is a functional receptor for the SARS coronavirus. *Nature* 426:450–454. <http://dx.doi.org/10.1038/nature02145>.
5. Raj VS, Mou H, Smits SL, Dekkers DH, Muller MA, Dijkman R, Muth D, Demmers JA, Zaki A, Fouchier RA, Thiel V, Drosten C, Rottier PJ, Osterhaus AD, Bosch BJ, Haagmans BL. 2013. Dipeptidyl peptidase 4 is a functional receptor for the emerging human coronavirus-EMC. *Nature* 495:251–254. <http://dx.doi.org/10.1038/nature12005>.
6. Yang Y, Du L, Liu C, Wang L, Ma C, Tang J, Baric RS, Jiang S, Li F. 2014. Receptor usage and cell entry of bat coronavirus HKU4 provide insight into bat-to-human transmission of MERS coronavirus. *Proc Natl Acad Sci U S A* 111:12516–12521. <http://dx.doi.org/10.1073/pnas.1405889111>.
7. Yeager CL, Ashmun RA, Williams RK, Cardellicchio CB, Shapiro LH, Look AT, Holmes KV. 1992. Human aminopeptidase N is a receptor for human coronavirus 229E. *Nature* 357:420–422. <http://dx.doi.org/10.1038/357420a0>.
8. Williams RK, Jiang GS, Holmes KV. 1991. Receptor for mouse hepatitis virus is a member of the carcinoembryonic antigen family of glycoproteins. *Proc Natl Acad Sci U S A* 88:5533–5536. <http://dx.doi.org/10.1073/pnas.88.13.5533>.
9. Babcock GJ, Eshaki DJ, Thomas WD, Jr, Ambrosino DM. 2004. Amino acids 270 to 510 of the severe acute respiratory syndrome coronavirus spike protein are required for interaction with receptor. *J Virol* 78:4552–4560. <http://dx.doi.org/10.1128/JVI.78.9.4552-4560.2004>.
10. Wong SK, Li W, Moore MJ, Choe H, Farzan M. 2004. A 193-amino acid fragment of the SARS coronavirus S protein efficiently binds angiotensin-converting enzyme 2. *J Biol Chem* 279:3197–3201.
11. Li F, Berardi M, Li W, Farzan M, Dormitzer PR, Harrison SC. 2006. Conformational states of the severe acute respiratory syndrome coronavirus spike protein ectodomain. *J Virol* 80:6794–6800. <http://dx.doi.org/10.1128/JVI.02744-05>.
12. Harrison SC. 2015. Viral membrane fusion. *Virology* 479–480:498–507.
13. White JM, Delos SE, Brecher M, Schornberg K. 2008. Structures and mechanisms of viral membrane fusion proteins: multiple variations on a common theme. *Crit Rev Biochem Mol Biol* 43:189–219. <http://dx.doi.org/10.1080/10409230802058320>.
14. Bertram S, Glowacka I, Muller MA, Lavender H, Gnirss K, Nehlmeier I, Niemeyer D, He Y, Simmons G, Drosten C, Soilleux EJ, Jahn O, Steffen I, Pohlmann S. 2011. Cleavage and activation of the severe acute respiratory syndrome coronavirus spike protein by human airway trypsin-like protease. *J Virol* 85:13363–13372. <http://dx.doi.org/10.1128/JVI.05300-11>.
15. Millet JK, Whittaker GR. 2014. Host cell entry of Middle East respiratory syndrome coronavirus after two-step, furin-mediated activation of the spike protein. *Proc Natl Acad Sci U S A* 111:15214–15219. <http://dx.doi.org/10.1073/pnas.1407087111>.
16. Belouzard S, Madu I, Whittaker GR. 2010. Elastase-mediated activation of the severe acute respiratory syndrome coronavirus spike protein at

- discrete sites within the S2 domain. *J Biol Chem* 285:22758–22763. <http://dx.doi.org/10.1074/jbc.M110.103275>.
17. Simmons G, Reeves JD, Rennekamp AJ, Amberg SM, Piefer AJ, Bates P. 2004. Characterization of severe acute respiratory syndrome-associated coronavirus (SARS-CoV) spike glycoprotein-mediated viral entry. *Proc Natl Acad Sci U S A* 101:4240–4245. <http://dx.doi.org/10.1073/pnas.0306446101>.
 18. Watanabe R, Matsuyama S, Shirato K, Maejima M, Fukushi S, Morikawa S, Taguchi F. 2008. Entry from the cell surface of severe acute respiratory syndrome coronavirus with cleaved S protein as revealed by pseudotype virus bearing cleaved S protein. *J Virol* 82:11985–11991. <http://dx.doi.org/10.1128/JVI.01412-08>.
 19. Bertram S, Dijkman R, Habjan M, Heurich A, Gierer S, Glowacka I, Welsch K, Winkler M, Schneider H, Hofmann-Winkler H, Thiel V, Pohlmann S. 2013. TMPRSS2 activates the human coronavirus 229E for cathepsin-independent host cell entry and is expressed in viral target cells in the respiratory epithelium. *J Virol* 87:6150–6160. <http://dx.doi.org/10.1128/JVI.03372-12>.
 20. Glowacka I, Bertram S, Muller MA, Allen P, Soilleux E, Pfeifferle S, Steffen I, Tsegaye TS, He Y, Gnirss K, Niemeyer D, Schneider H, Drosten C, Pohlmann S. 2011. Evidence that TMPRSS2 activates the severe acute respiratory syndrome coronavirus spike protein for membrane fusion and reduces viral control by the humoral immune response. *J Virol* 85:4122–4134. <http://dx.doi.org/10.1128/JVI.02232-10>.
 21. Gallaher WR. 1996. Similar structural models of the transmembrane proteins of Ebola and avian sarcoma viruses. *Cell* 85:477–478. [http://dx.doi.org/10.1016/S0092-8674\(00\)81248-9](http://dx.doi.org/10.1016/S0092-8674(00)81248-9).
 22. Hernandez LD, White JM. 1998. Mutational analysis of the candidate internal fusion peptide of the avian leukosis and sarcoma virus subgroup A envelope glycoprotein. *J Virol* 72:3259–3267.
 23. Delos SE, Gilbert JM, White JM. 2000. The central proline of an internal viral fusion peptide serves two important roles. *J Virol* 74:1686–1693. <http://dx.doi.org/10.1128/JVI.74.4.1686-1693.2000>.
 24. Sanchez A, Yang ZY, Xu L, Nabel GJ, Crews T, Peters CJ. 1998. Biochemical analysis of the secreted and virion glycoproteins of Ebola virus. *J Virol* 72:6442–6447.
 25. Cross KJ, Langley WA, Russell RJ, Skehel JJ, Steinhauer DA. 2009. Composition and functions of the influenza fusion peptide. *Protein Pept Lett* 16:766–778. <http://dx.doi.org/10.2174/092986609788681715>.
 26. Gallaher WR. 1987. Detection of a fusion peptide sequence in the transmembrane protein of human immunodeficiency virus. *Cell* 50:327–328. [http://dx.doi.org/10.1016/0092-8674\(87\)90485-5](http://dx.doi.org/10.1016/0092-8674(87)90485-5).
 27. Martin I, Ruyschaert JM. 2000. Common properties of fusion peptides from diverse systems. *Biosci Rep* 20:483–500. <http://dx.doi.org/10.1023/A:1010454803579>.
 28. Guillen J, de Almeida RF, Prieto M, Villalain J. 2008. Structural and dynamic characterization of the interaction of the putative fusion peptide of the S2 SARS-CoV virus protein with lipid membranes. *J Phys Chem B* 112:6997–7007.
 29. Guillen J, Kinnunen PK, Villalain J. 2008. Membrane insertion of the three main membranotropic sequences from SARS-CoV S2 glycoprotein. *Biochim Biophys Acta* 1778:2765–2774. <http://dx.doi.org/10.1016/j.bbame.2008.07.021>.
 30. Guillen J, Perez-Berna AJ, Moreno MR, Villalain J. 2005. Identification of the membrane-active regions of the severe acute respiratory syndrome coronavirus spike membrane glycoprotein using a 16/18-mer peptide scan: implications for the viral fusion mechanism. *J Virol* 79:1743–1752. <http://dx.doi.org/10.1128/JVI.79.3.1743-1752.2005>.
 31. Guillen J, Perez-Berna AJ, Moreno MR, Villalain J. 2008. A second SARS-CoV S2 glycoprotein internal membrane-active peptide. Biophysical characterization and membrane interaction. *Biochemistry* 47:8214–8224.
 32. Madu IG, Roth SL, Belouard S, Whittaker GR. 2009. Characterization of a highly conserved domain within the severe acute respiratory syndrome coronavirus spike protein S2 domain with characteristics of a viral fusion peptide. *J Virol* 83:7411–7421. <http://dx.doi.org/10.1128/JVI.00079-09>.
 33. Sainz B, Jr, Rausch JM, Gallaher WR, Garry RF, Wimley WC. 2005. Identification and characterization of the putative fusion peptide of the severe acute respiratory syndrome-associated coronavirus spike protein. *J Virol* 79:7195–7206. <http://dx.doi.org/10.1128/JVI.79.11.7195-7206.2005>.
 34. Luo Z, Weiss SR. 1998. Roles in cell-to-cell fusion of two conserved hydrophobic regions in the murine coronavirus spike protein. *Virology* 244:483–494. <http://dx.doi.org/10.1006/viro.1998.9121>.
 35. Chambers P, Pringle CR, Easton AJ. 1990. Heptad repeat sequences are located adjacent to hydrophobic regions in several types of virus fusion glycoproteins. *J Gen Virol* 71(Part 12):3075–3080. <http://dx.doi.org/10.1099/0022-1317-71-12-3075>.
 36. Jeffers SA, Tusell SM, Gillim-Ross L, Hemmila EM, Achenbach JE, Babcock GJ, Thomas WD, Jr, Thackray LB, Young MD, Mason RJ, Ambrosino DM, Wentworth DE, Demartini JC, Holmes KV. 2004. CD209L (L-SIGN) is a receptor for severe acute respiratory syndrome coronavirus. *Proc Natl Acad Sci U S A* 101:15748–15753. <http://dx.doi.org/10.1073/pnas.0403812101>.
 37. Qian Z, Dominguez SR, Holmes KV. 2013. Role of the spike glycoprotein of human Middle East respiratory syndrome coronavirus (MERS-CoV) in virus entry and syncytia formation. *PLoS One* 8:e76469. <http://dx.doi.org/10.1371/journal.pone.0076469>.
 38. Peng G, Sun D, Rajashankar KR, Qian Z, Holmes KV, Li F. 2011. Crystal structure of mouse coronavirus receptor-binding domain complexed with its murine receptor. *Proc Natl Acad Sci U S A* 108:10696–10701. <http://dx.doi.org/10.1073/pnas.1104306108>.
 39. Zelus BD, Schickli JH, Blau DM, Weiss SR, Holmes KV. 2003. Conformational changes in the spike glycoprotein of murine coronavirus are induced at 37 degrees C either by soluble murine CEACAM1 receptors or by pH 8. *J Virol* 77:830–840. <http://dx.doi.org/10.1128/JVI.77.2.830-840.2003>.
 40. Qian Z, Wang H, Empig C, Anderson WF, Albritton LM. 2004. Complementation of a binding-defective retrovirus by a host cell receptor mutant. *J Virol* 78:5766–5772. <http://dx.doi.org/10.1128/JVI.78.11.5766-5772.2004>.
 41. Martin I, Schaal H, Scheid A, Ruyschaert JM. 1996. Lipid membrane fusion induced by the human immunodeficiency virus type 1 gp41 N-terminal extremity is determined by its orientation in the lipid bilayer. *J Virol* 70:298–304.
 42. Chen YH, Yang JT, Chau KH. 1974. Determination of the helix and beta form of proteins in aqueous solution by circular dichroism. *Biochemistry* 13:3350–3359. <http://dx.doi.org/10.1021/bi00713a027>.
 43. Hope MJ, Bally MB, Webb G, Cullis PR. 1985. Production of large unilamellar vesicles by a rapid extrusion procedure: characterization of size distribution, trapped volume and ability to maintain a membrane potential. *Biochim Biophys Acta* 812:55–65. [http://dx.doi.org/10.1016/0005-2736\(85\)90521-8](http://dx.doi.org/10.1016/0005-2736(85)90521-8).
 44. Struck DK, Hoekstra D, Pagano RE. 1981. Use of resonance energy transfer to monitor membrane fusion. *Biochemistry* 20:4093–4099. <http://dx.doi.org/10.1021/bi00517a023>.
 45. Gierer S, Bertram S, Kaup F, Wrensche F, Heurich A, Kramer-Kuhl A, Welsch K, Winkler M, Meyer B, Drosten C, Dittmer U, von Hahn T, Simmons G, Hofmann H, Pohlmann S. 2013. The spike protein of the emerging betacoronavirus EMC uses a novel coronavirus receptor for entry, can be activated by TMPRSS2, and is targeted by neutralizing antibodies. *J Virol* 87:5502–5511. <http://dx.doi.org/10.1128/JVI.00128-13>.
 46. Waring AJ, Mobley PW, Gordon LM. 1998. Conformational mapping of a viral fusion peptide in structure-promoting solvents using circular dichroism and electrospray mass spectrometry. *Proteins* 2:38–49.
 47. Nelson JW, Kallenbach NR. 1986. Stabilization of the ribonuclease S-peptide alpha-helix by trifluoroethanol. *Proteins* 1:211–217. <http://dx.doi.org/10.1002/prot.340010303>.
 48. Gao J, Lu G, Qi J, Li Y, Wu Y, Deng Y, Geng H, Li H, Wang Q, Xiao H, Tan W, Yan J, Gao GF. 2013. Structure of the fusion core and inhibition of fusion by a heptad repeat peptide derived from the S protein of Middle East respiratory syndrome coronavirus. *J Virol* 87:13134–13140. <http://dx.doi.org/10.1128/JVI.02433-13>.
 49. Lu L, Liu Q, Zhu Y, Chan KH, Qin L, Li Y, Wang Q, Chan JF, Du L, Yu F, Ma C, Ye S, Yuen KY, Zhang R, Jiang S. 2014. Structure-based discovery of Middle East respiratory syndrome coronavirus fusion inhibitor. *Nat Commun* 5:3067.
 50. Bosch BJ, Martina BE, Van Der Zee R, Lepault J, Haijema BJ, Versluis C, Heck AJ, De Groot R, Osterhaus AD, Rottier PJ. 2004. Severe acute respiratory syndrome coronavirus (SARS-CoV) infection inhibition using spike protein heptad repeat-derived peptides. *Proc Natl Acad Sci U S A* 101:8455–8460. <http://dx.doi.org/10.1073/pnas.0400576101>.
 51. Xu Y, Liu Y, Lou Z, Qin L, Li X, Bai Z, Pang H, Tien P, Gao GF, Rao Z. 2004. Structural basis for coronavirus-mediated membrane fusion.

- Crystal structure of mouse hepatitis virus spike protein fusion core. *J Biol Chem* 279:30514–30522.
52. Xu Y, Lou Z, Liu Y, Pang H, Tien P, Gao GF, Rao Z. 2004. Crystal structure of severe acute respiratory syndrome coronavirus spike protein fusion core. *J Biol Chem* 279:49414–49419. <http://dx.doi.org/10.1074/jbc.M408782200>.
 53. Bosch BJ, van der Zee R, de Haan CA, Rottier PJ. 2003. The coronavirus spike protein is a class I virus fusion protein: structural and functional characterization of the fusion core complex. *J Virol* 77:8801–8811. <http://dx.doi.org/10.1128/JVI.77.16.8801-8811.2003>.
 54. Kaufman G, Liu P, Leibowitz JL. 2014. Identification of novel functional regions within the spike glycoprotein of MHV-A59 based on a bioinformatics approach. *Virus Res* 189:177–188. <http://dx.doi.org/10.1016/j.virusres.2014.05.023>.
 55. McRoy WC, Baric RS. 2008. Amino acid substitutions in the S2 subunit of mouse hepatitis virus variant V51 encode determinants of host range expansion. *J Virol* 82:1414–1424. <http://dx.doi.org/10.1128/JVI.01674-07>.
 56. Liao Y, Zhang SM, Neo TL, Tam JP. 2015. Tryptophan-dependent membrane interaction and heteromerization with the internal fusion peptide by the membrane proximal external region of SARS-CoV spike protein. *Biochemistry* 54:1819–1830. <http://dx.doi.org/10.1021/bi501352u>.
 57. Li L, Vorobyov I, MacKerell AD, Jr, Allen TW. 2008. Is arginine charged in a membrane? *Biophys J* 94:L11–L13. <http://dx.doi.org/10.1529/biophysj.107.121566>.
 58. Lai AL, Park H, White JM, Tamm LK. 2006. Fusion peptide of influenza hemagglutinin requires a fixed angle boomerang structure for activity. *J Biol Chem* 281:5760–5770.
 59. Li J, Das P, Zhou R. 2010. Single mutation effects on conformational change and membrane deformation of influenza hemagglutinin fusion peptides. *J Phys Chem B* 114:8799–8806. <http://dx.doi.org/10.1021/jp1029163>.
 60. Li Y, Han X, Lai AL, Bushweller JH, Cafiso DS, Tamm LK. 2005. Membrane structures of the hemifusion-inducing fusion peptide mutant G1S and the fusion-blocking mutant G1V of influenza virus hemagglutinin suggest a mechanism for pore opening in membrane fusion. *J Virol* 79:12065–12076. <http://dx.doi.org/10.1128/JVI.79.18.12065-12076.2005>.
 61. Lai AL, Freed JH. 2014. HIV gp41 fusion peptide increases membrane ordering in a cholesterol-dependent fashion. *Biophys J* 106:172–181. <http://dx.doi.org/10.1016/j.bpj.2013.11.027>.
 62. Fuhrmans M, Marrink SJ. 2012. Molecular view of the role of fusion peptides in promoting positive membrane curvature. *J Am Chem Soc* 134:1543–1552. <http://dx.doi.org/10.1021/ja207290b>.
 63. Gregory SM, Harada E, Liang B, Delos SE, White JM, Tamm LK. 2011. Structure and function of the complete internal fusion loop from Ebola virus glycoprotein 2. *Proc Natl Acad Sci U S A* 108:11211–11216. <http://dx.doi.org/10.1073/pnas.1104760108>.
 64. Lau WL, Ege DS, Lear JD, Hammer DA, DeGrado WF. 2004. Oligomerization of fusogenic peptides promotes membrane fusion by enhancing membrane destabilization. *Biophys J* 86:272–284. [http://dx.doi.org/10.1016/S0006-3495\(04\)74103-X](http://dx.doi.org/10.1016/S0006-3495(04)74103-X).
 65. Yang J, Prorok M, Castellino FJ, Weliky DP. 2004. Oligomeric beta-structure of the membrane-bound HIV-1 fusion peptide formed from soluble monomers. *Biophys J* 87:1951–1963. <http://dx.doi.org/10.1529/biophysj.103.028530>.
 66. Chang DK, Cheng SF, Kantchev EA, Lin CH, Liu YT. 2008. Membrane interaction and structure of the transmembrane domain of influenza hemagglutinin and its fusion peptide complex. *BMC Biol* 6:2. <http://dx.doi.org/10.1186/1741-7007-6-2>.
 67. Donald JE, Zhang Y, Fiorin G, Carnevale V, Slochower DR, Gai F, Klein ML, DeGrado WF. 2011. Transmembrane orientation and possible role of the fusogenic peptide from parainfluenza virus 5 (PIV5) in promoting fusion. *Proc Natl Acad Sci U S A* 108:3958–3963. <http://dx.doi.org/10.1073/pnas.1019668108>.
 68. Reuven EM, Dadon Y, Viard M, Manukovsky N, Blumenthal R, Shai Y. 2012. HIV-1 gp41 transmembrane domain interacts with the fusion peptide: implication in lipid mixing and inhibition of virus-cell fusion. *Biochemistry* 51:2867–2878. <http://dx.doi.org/10.1021/bi201721r>.
 69. Teese MG, Langosch D. 2015. Role of GxxxG motifs in transmembrane domain interactions. *Biochemistry* 54:5125–5135. <http://dx.doi.org/10.1021/acs.biochem.5b00495>.
 70. Faingold O, Cohen T, Shai Y. 2012. A GxxxG-like motif within HIV-1 fusion peptide is critical to its immunosuppressant activity, structure, and interaction with the transmembrane domain of the T-cell receptor. *J Biol Chem* 287:33503–33511. <http://dx.doi.org/10.1074/jbc.M112.370817>.
 71. Chang DK, Cheng SF, Chien WJ. 1997. The amino-terminal fusion domain peptide of human immunodeficiency virus type 1 gp41 inserts into the sodium dodecyl sulfate micelle primarily as a helix with a conserved glycine at the micelle-water interface. *J Virol* 71:6593–6602.
 72. Sackett K, Shai Y. 2005. The HIV fusion peptide adopts intermolecular parallel beta-sheet structure in membranes when stabilized by the adjacent N-terminal heptad repeat: a 13C FTIR study. *J Mol Biol* 350:790–805. <http://dx.doi.org/10.1016/j.jmb.2005.05.030>.
 73. Lorieau JL, Louis JM, Bax A. 2010. The complete influenza hemagglutinin fusion domain adopts a tight helical hairpin arrangement at the lipid-water interface. *Proc Natl Acad Sci U S A* 107:11341–11346. <http://dx.doi.org/10.1073/pnas.1006142107>.
 74. Haria NR, Monticelli L, Fraternali F, Lorenz CD. 2014. Plasticity and conformational equilibria of influenza fusion peptides in model lipid bilayers. *Biochim Biophys Acta* 1838:1169–1179. <http://dx.doi.org/10.1016/j.bbmem.2013.12.020>.